Published in final edited form as:
Mol Cancer Ther. 2020 February 01; 19(2): 637–649. doi:10.1158/1535-7163.MCT-19-0330.

A Synergistic Anti-Cancer FAK and HDAC Inhibitor Combination Discovered by a Novel Chemical-Genetic High-Content Phenotypic Screen

John C. Dawson[#1], **Bryan Serrels**[#1], **Adam Byron**[#1], **Morwenna T. Muir**[1], **Ashraff Makda**[1], **Amaya García-Muñoz**[2], **Alex von Kriegsheim**[1,2], **Daniel Lietha**[3], **Neil O. Carragher**[1,†], **Margaret C. Frame**[1,†]

[1]Cancer Research UK Edinburgh Centre, Institute of Genetics and Molecular Medicine, University of Edinburgh, Edinburgh, United Kingdom

[2]Systems Biology Ireland, University College Dublin, Dublin, Ireland

[3]Cell Signaling and Adhesion Group, Structural Biology Program, Spanish National Cancer Research Centre (CNIO), Madrid, Spain

[#] These authors contributed equally to this work.

Abstract

We mutated the focal adhesion kinase (FAK) catalytic domain to inhibit binding of the chaperone Cdc37 and ATP, mimicking the actions of a FAK kinase inhibitor. We re-expressed mutant and wild-type FAK in squamous cell carcinoma (SCC) cells from which endogenous FAK had been deleted, genetically fixing one axis of a FAK inhibitor combination high-content phenotypic screen to discover drugs that may synergize with FAK inhibitors. Histone deacetylase (HDAC) inhibitors represented the major class of compounds that potently induced multiparametric phenotypic changes when FAK was rendered kinase-defective or inhibited pharmacologically in SCC cells. Combined FAK and HDAC inhibitors arrest proliferation and induce apoptosis in a sub-set of cancer cell lines in vitro and efficiently inhibit their growth as tumors in vivo. Mechanistically, HDAC inhibitors potentiate inhibitor-induced FAK inactivation and impair FAK-associated nuclear YAP in sensitive cancer cell lines. Here we report the discovery of a new, clinically actionable, synergistic combination between FAK and HDAC inhibitors.

Keywords

Focal Adhesion Kinase; Histone Deacetylase; Inhibitor; Drug Combination; Cancer; High-Content Phenotypic Screening

[†]Corresponding authors: Margaret C. Frame, Cancer Research UK Edinburgh Centre, Institute of Genetics and Molecular Medicine, University of Edinburgh, Crewe Road South, Edinburgh EH4 2XR, United Kingdom. Phone: +44 (0)131 651 8510; m.frame@ed.ac.uk; Neil O. Carragher, Cancer Research UK Edinburgh Centre, Institute of Genetics and Molecular Medicine, University of Edinburgh, Crewe Road South, Edinburgh EH4 2XR, United Kingdom. Phone: +44 (0)131 651 8690; n.carragher@ed.ac.uk.

Conflict of Interest Statement: M. C. Frame and N. O. Carragher are members of the scientific advisory board and shareholders in Amplia Therapeutics Limited.

Europe PMC Funders Author Manuscripts

Introduction

Focal adhesion kinase (FAK) is a non-receptor tyrosine kinase that is frequently over-expressed in cancer, where it functions downstream of integrins and growth factor receptors to regulate a diverse range of cellular functions, including survival, proliferation, adhesion, migration, angiogenesis, stemness, and more recently, cytokine expression (1,2). FAK plays a pivotal role in transducing signals from the plasma membrane and the nucleus (2–8). It is recognized as a high-value druggable target for cancer therapy, resulting in the development of multiple FAK kinase inhibitors that are being tested in clinical trials (reviewed in (1)). We have argued that FAK inhibitors may best be used in combination with other agents because FAK is part of key survival pathways, including when cancer cells are exposed to stress or treated in combination with anti-cancer agents such as BRAF or autophagy inhibitors (4,5,9). Potent FAK inhibitors have been generated (BI 853520, GSK2256098, TAE226, VS-4718, VS-6062), with efficacy in clinical trials largely restricted to stabilized disease (10,11). The FAK inhibitors VS-6063 and GSK2256098 are currently being evaluated clinically in combination with inhibitors targeting Raf/MEK (RO5126766 and trametinib), the checkpoint blockade inhibitor anti-PD-1 (pembrolizumab), and the chemotherapeutic drugs paclitaxel, carboplatin, and gemcitabine (ClinicalTrials.gov). Here we report a new chemical-genetic phenotypic screening approach to identify combinations between FAK, and other, targeted inhibitors.

Cdc37 is a protein kinase-specific co-chaperone for Hsp90 which binds to approximately 60% of kinases encoded by the mammalian kinome (12). The Hsp90-Cdc37 complex binds to inactive kinases to ensure their correct folding, transport, and degradation, and therefore targeting of this complex is being explored as a tractable therapeutic targeting strategy for the treatment of cancer (reviewed in (13)). Traditional ATP-competitive kinase inhibitors have been shown to inhibit the binding of Cdc37, resulting in kinase inhibition and degradation via the proteasome (14). Cdc37 prevents client kinases from binding ATP by interacting with the glycine-rich loop of the client kinase domain, which is essential for ATP binding, effectively inhibiting kinase activation (15,16). Mutation of the Cdc37 binding site in the client kinase domain glycine-rich loop also blocks ATP binding (14–16). Therefore, we used a mutant FAK protein that could not bind Cdc37 (see details below) as a means to mimic FAK bound to an inhibitor, and to genetically fix one axis of a chemical-genetic phenotypic screen.

We used a multiparametric, high-content phenotypic screening approach that permits unbiased “morphometric profiling” of compound activity and quantification of functional similarities and dissimilarities between drug mechanisms of action (MOAs) across distinct cell types (17–20). Integration of information-rich phenotypic assays (as opposed to information-poor “black-box” phenotypic assays) with the latest advances in multiparametric image analysis, multivariate statistics, and new image informatics tools, permits the classification of compound-induced morphometric phenotypes (21,22).

Phenotypic “fingerprints” derived from multiparametric, high-content morphometric measurements were used here to identify clusters enriched with specific compound MOA and target classes which, when perturbed, induced a characteristic phenotypic response

between cell lines that differed only in FAK activity. In this way, we combined high-content phenotypic screening with cancer cells genetically modified to express a new discriminatory FAK mutant protein (described below) to identify synergistic FAK inhibitor combinations. For this, we generated a novel kinase-defective FAK protein (FAK-G431A,F433A) that abolished binding of the Cdc37 chaperone protein and ATP. This FAK-G431A,F433A mutant behaved, in many respects, including Cdc37 binding, more like FAK in the presence of a small-molecule FAK inhibitor when it was compared to a conventional kinase-defective FAK mutant (FAK-KD) (23). We re-expressed FAK-G431A,F433A in squamous cell carcinoma (SCC) cells from which the *Fak* gene (*Ptk2*) had been previously deleted by Cre-lox-mediated recombination (as we have described before (2,5,24)), allowing us to compare the loss of FAK's kinase activity with cells that do not express FAK (FAK−/−) or that re-express wild-type FAK (FAK-WT). This allowed us to genetically fix one axis of a multiparametric phenotypic screen; from this, we identified distinct phenotypic responses between cells expressing FAK-WT and FAK-G431A,F433A after treatment with histone deacetylase (HDAC) inhibitors, indicative of synergism. This synergy was confirmed by combining pharmacological FAK kinase and HDAC inhibitors in subsequent dose-ratio combination matrix experiments. In screening multiple cell lines, we identified a sub-set of cancer cells in which FAK and HDAC inhibitors synergized to inhibit proliferation. In these, HDAC inhibitors enhanced FAK inhibitor-induced FAK inactivation as judged by FAK-Y397 autophosphorylation, and this was linked to enhanced nuclear exclusion of YES-associated protein (YAP) in vitro and in vivo, suggesting that combining FAK and HDAC inhibitors promotes dysregulation of Hippo/YAP signaling.

Materials and Methods

Compounds and antibodies

VS-4718 (#S7653), VS-6063 (#S7654), PF-562,271 (#S2890), GSK2256098 (#S8523), vorinostat (#S1047), panobinostat (#S1030), staurosporine (#S1421), and paclitaxel (#S1150) were purchased from Selleck Chemicals. Chemical structures are shown for the FAK kinase inhibitors (VS-4718, VS-6063, PF-562,271, and GSK2256098) and HDAC inhibitors (vorinostat and panobinostat) in Supplementary Fig. 1A. Compound libraries were from BioAscent. Antibodies used were purchased from Cell Signaling Technology (FAK phosphorylated tyrosine-(pY)397, #3283; FAK, #3285; GAPDH, #2118; YAP, #14074; YAP phosphorylated serine-(pS)127, #13008; histone H3, #9715; histone H3 acetylated lysine-56 (K-Ac), #4243; Cdc37, #4793; Cdc37 pS13, #13248; Src, #2109; Axl #8661) or Abcam (YAP, #EP1674Y).

Cell lines

The murine SCC FAK cell model was generated, isolated, and grown as previously described (6). The Cdc37 binding site in the glycine-rich loop of the FAK kinase domain was mutated using previously published mutations of other published Cdc37 kinase binding sites (15,16). SCC FAK−/− cells stably re-expressing FAK-WT, FAK-KD, or FAK-G431A,F433A were maintained under selection using 0.25 mg/mL hygromycin (Invivogen; #ant-hg-1). Human cell lines were cultured in RPMI (Sigma-Aldrich; #R0883) supplemented with 2 mmol/L L-glutamine (Thermo Fisher Scientific; #25030081) and 10%

FBS. Human cell lines were purchased from ATCC, and esophageal cells were a gift of T. R. Hupp (University of Edinburgh). Cell lines were routinely tested for mycoplasma (twice yearly) and cell line authenticity confirmed by STR profiling where appropriate. Primary dermal fibroblasts were cultured from skin punch biopsies in DMEM (Thermo Fisher Scientific; #11960044) supplemented with 10% FBS and 2 mmol/L L-glutamine and used for experiments at passages 3 and 4.

Subcutaneous tumor growth

Experiments involving animals were carried out in accordance with the UK Coordinating Committee on Cancer Research guidelines by approved protocol (HO PL 70/8897). SCC FAK-WT cells (0.25×10^6), A549 cells (5×10^6), or Flo1 cells (5×10^6) were injected subcutaneously on each flank of CD1-nude or NSG (Flo1) mice (5 per group). Established tumor-bearing mice were randomized into treatment groups and dosed with panobinostat (5 mg/kg) 5 days out of 7 by IP injection (for a total of 14 injections) and twice daily with VS-4718 by oral gavage. Panobinostat was dissolved in DMSO and diluted in 10% PEG 400/1% Tween 80 immediately prior to injection. VS-4718 was prepared in 0.5% hydroxypropyl methylcellulose. Tumor growth was monitored by caliper measurements and tumor volume calculated using the formula $V = (W^2 \times L)/2$, where V is tumor volume, W is tumor width, and L is tumor length. Animals were sacrificed when tumors reached their maximum allowable size or when tumor ulceration occurred.

Immunoprecipitation and immunoblot analyses

Cell lysates were prepared for immunoblotting and immunoprecipitation as previously described (3,7).

Reverse-phase protein array (RPPA) analysis

Flo1 cell lysates from 24-hour drug-treated cells were isolated in RIPA as described above and processed for RPPA (25) by the IGMM Protein and Antibody Microarray Facility (Cancer Research UK Edinburgh Centre, University of Edinburgh).

Immunofluorescence

Cells were grown on glass coverslips and processed as previously described (5).

FAK mutant combination screen

SCC cells were seeded in collagen I-coated 384-well optical bottom plates (Greiner; #781091) at 300 cells per well. Cells were cultured for 24 hours before addition of compounds using a BioMek FX liquid handling station for a further 24 hours. Plates were fixed with 4% paraformaldehyde in PBS for 20 minutes, followed by washing with PBS twice and incubation with blocking solution (0.2% Triton X-100, 1% BSA in PBS) for 30 minutes. Plates were incubated with Alexa Fluor 488-labeled phalloidin (1:250; Cell Signaling Technology; #8878) and Hoechst 33345 (2 μg/mL; Molecular Probes; #H1399) made up in blocking solution for 50 minutes. Finally, an equal volume of High-Content Screening (HCS) CellMask deep red (1:75,000; Molecular Probes; #H32721) diluted in blocking solution was added for 10 minutes. Plates were washed with PBS and plates

sealed. Six images per well were acquired using an ImageXpress Micro XLS widefield microscope (Molecular Devices) with a 20× S Plan Fluor objective, with typically 150–200 cells per image of control wells. Each plate contained 32 wells treated with 0.1% DMSO as a negative control and 16 wells treated with paclitaxel (300 nmol/L) and 16 wells with staurosporine (300 nmol/L) as positive controls. Images were quantified using CellProfiler (26) and MetaXpress software (Molecular Devices) (Supplementary Text).

YAP localization analysis

Cells in 384-well plates were fixed with 4% paraformaldehyde for 20 minutes. Plates were washed with PBS and cells permeabilized and blocked (0.3% Triton X-100, 2.5% FBS in PBS) for 30 minutes. Plates were immunolabeled with anti-YAP antibody (Abcam; #EP1674Y) diluted in blocking buffer and incubated at 4°C overnight. Plates were washed with PBS and labeled with anti-rabbit Alexa Fluor 594-conjugated secondary antibody and Hoechst (2 μg/mL) diluted in blocking buffer. Plates were washed in PBS and sealed. Nine images per well were acquired using an ImageXpress Micro XLS widefield microscope with a 20× S Plan Fluor objective, with typically 100–200 cells per image and 6 replicate wells per condition per plate. Images were quantified using CellProfiler (Supplementary Text).

Live-cell kinetic analysis of cell cycle

SCC FAK-WT cells stably expressing the FUCCI cell cycle reporter (3) were seeded in 96-well collagen I-coated plates. Cells were treated with drug combinations in a dose matrix and plates monitored in an IncuCyte Zoom microscope (Essen BioScience) at 37°C over 5 days. Images were analyzed using the inbuilt analysis software.

Apoptosis assay

Cells were seeded in 96-well plates with IncuCyte Caspase-3/7 Green Apoptosis Assay reagent (Essen BioScience; #4440) and treated with compounds. Plates were imaged in an IncuCyte Zoom microscope, acquiring images every 3 hours over a 72-hour period using the ‘phase’ and ‘green’ channels. Images were analyzed using the IncuCyte Zoom software, and apoptosis was expressed as a percentage of the population.

Generation of spheroids

Cells were seeded in 96-well ultra-low-attachment “U” bottom plates (Corning; #7007) at 2000 cells per well in normal growth medium and centrifuged at 1000 × *g*. Cells were allowed to form a single spheroid per well over 3 days, after which they were drug treated and monitored over 14 days for using an ImageXpress Micro XLS widefield microscope. For assessment of spheroid viability, spheroids were incubated with calcein AM (4 μmol/L final concentration; Molecular Probes; #C3099) for 1 hour prior to imaging.

Immunohistochemistry

For immunohistochemistry, reagents were from DAKO using standard procedures. Briefly, tumor sections (4 μm thickness) were rehydrated, and antigen retrieval was performed using boiling citrate buffer (pH 6.0) for 5 minutes. Endogenous peroxidase activity was blocked using peroxidase blocking solution (#S2023) and then sections were incubated with serum-

free blocking solution (#X0909). Sections were incubated with diluted primary antibody overnight at 4°C. Sections were washed in TBS and incubated with secondary (#P0448) for 30 minutes. Sections were washed in TBS and incubated with DAB reagent (#K3468) for 5 minutes, and finally, sections were counter-stained with eosin, dehydrated, and mounted using DPX mounting medium (#44581). Images were acquired on a Hamamatsu NanoZoomer using a 40x objective, and tumors were analyzed using QuPath analysis software (27). Tumor margins were defined as a band of tumor cells 200 μm wide around the tumor edge.

Cell viability assay

Cells were seeded in 96-well plates at 2000 cells per well and incubated for 24 hours before treatment. Cells were incubated with compounds for 72 hours; untreated cells were incubated with 0.1% DMSO. Alamar Blue (Invitrogen; #DAL1025) was added to each well and plates incubated for 3 hours. Fluorescence emission was read on an EnVision 2101 multilabel plate reader (PerkinElmer; excitation = 540 nm, emission = 590 nm). All conditions were normalized to plate DMSO control wells.

Colony formation assay

Single cells (1000 per well) were seeded in six-well plates, treated with drugs, and allowed to grow over 7–10 days. Plates were washed with PBS and colonies stained with Coomassie Blue (0.25 g/L Coomassie Brilliant Blue R-250 (#27816) made up in 45% water, 45% acetic acid, and 10% methanol). The colony area covering the well was quantified using ImageJ (National Institutes of Health).

Synergy calculation

Normalized measurements were averaged (n from ≥ 3 independent experiments) and analyzed using SynergyFinder (28) using the Bliss, Loewe, and ZIP synergy models.

Metabolic labeling

SCC cells were cultured in SILAC MEM (DC Biosciences) containing either L-[U-$^{13}C_6$]arginine and L-[$^{2}H_4$]lysine (R6K4; medium label) or unlabeled L-arginine and unlabeled L-lysine (R0K0; light label) for more than six cell doublings. At time t = 0 h, cells were washed twice in warm PBS, and either 1×10^6 light-labeled cells were re-plated in light-labeled medium or 1×10^6 medium-labeled cells were re-plated in SILAC MEM containing L-[U-$^{13}C_6$,$^{15}N_4$]arginine and L-[U-$^{13}C_6$,$^{15}N_2$]lysine (R10K8; heavy label). SILAC MEM was supplemented with 10% dialyzed FBS, 2 mmol/L L-glutamine, 1 mmol/L sodium pyruvate, MEM vitamins, and MEM non-essential amino acids throughout the experiments. Cells were harvested and lysed in RIPA buffer (as above) at t = 0.5, 6, 20, 45, and 70 h. Light-labeled cell lysates were mixed with medium-/heavy-labeled cell lysates at 1:1 ratio by total protein amount, mixed lysates were resolved by polyacrylamide gel electrophoresis, and gels were stained with InstantBlue (Expedeon).

Mass spectrometric analysis of immune complexes

For analysis of immune complexes using label-free mass spectrometry, captured proteins were subjected to on-bead proteolytic digestion, desalting, and liquid chromatography–tandem mass spectrometry, as previously described (29). Mean label-free quantification intensities were calculated from technical-duplicate mass spectrometry runs for each of three biological replicates per experimental condition using MaxQuant (version 1.5.6.5) (30), and peptide and protein false discovery rates were set to 1%. Label-free quantification intensities were binary-logarithm transformed and sample-median subtracted, and proteins quantified in fewer than half of all samples were excluded. Missing values were imputed from a width-compressed, down-shifted normal distribution using Perseus (version 1.5.2.6) (31). Statistical significance of differentially regulated FAK-binding proteins was determined by analysis of variance and two-tailed Student's t-tests with artificial within-groups variance set to 1 and a permutation-based false discovery rate threshold of 5% (applying 1000 randomizations).

Mass spectrometric analysis of FAK turnover

For FAK turnover profiling using SILAC-based mass spectrometry, gel portions spanning the molecular weight range 100–150 kDa of resolved mixed lysates (see above) were excised and subjected to in-gel proteolytic digestion, as previously described (32). Peptides were analyzed by liquid chromatography–tandem mass spectrometry, as previously described (33). Peptide and protein false discovery rates were set to 1%. SILAC ratios were calculated for each of three biological replicates per experimental condition. FAK synthesis and degradation curves were determined from normalized SILAC ratio profiles (heavy/light labels and medium/light labels, respectively) by nonlinear regression using Prism (GraphPad). Inferred FAK turnover time was calculated as the intersection between the synthesis and degradation curves (Supplementary Text).

Results

Characterization of a novel kinase-defective FAK that mimics pharmacological inhibition

We initially identified the protein kinase chaperone Cdc37 as a FAK binding partner (Fig. 1A; Supplementary Fig. S1B) and found that mutation of the Cdc37 binding site in the glycine-rich loop of the FAK kinase domain at glycine-(G)431 and phenylalanine-(F)433 to alanine (FAK-G431A,F433A) abolished Cdc37 binding, while a previously described kinase-inactivating mutation of FAK (K454R, FAK-KD (23)) did not (Fig. 1A). This mimicked the effect of ATP-competitive FAK kinase inhibitors, four of which blocked Cdc37 binding to FAK-WT (Fig. 1B). We confirmed that FAK-G431A,F433A was completely defective in kinase activity as measured by lack of any visible autophosphorylation at FAK-Y397 (Fig. 1C), presumably because the glycine-rich loop is required for ATP binding (14). Moreover, FAK-G431A,F433A impairs binding to Src (Fig. 1D), although it does not impair binding to kinase-independent partners, including the scaffold protein RACK1 (Supplementary Fig. S1C (8)). Further characterization revealed that Cdc37 co-localized with FAK at sites of focal adhesions, and loss of Cdc37 binding did not alter FAK's localization to focal adhesions (Fig. 1E and F). We noted that stable re-expression of FAK-G431A,F433A in SCC cells repeatedly resulted in lower expression

when compared with re-introduction of either FAK-WT or FAK-KD (Fig. 1A). If the FAK-G431A,F433A mutant was to be efficiently used to mimic effects of pharmacological FAK kinase inhibitors, it was important to determine whether the stability of FAK was affected by loss of Cdc37 binding, since Cdc37 is an Hsp90 co-chaperone protein that may influence protein turnover (12). Therefore, we quantified protein synthesis and degradation in SCC cells expressing FAK-WT and FAK-G431A,F433A using dynamic stable isotope labeling of amino acids in cell culture (SILAC) and mass spectrometry. We analyzed normalized SILAC ratio profiles derived from metabolically labeled FAK peptides, and inferred FAK turnover times indicated that loss of Cdc37 binding did not significantly affect FAK-G431A,F433A protein turnover when compared to FAK-WT (Fig. 1G; Supplementary Fig. S1D).

To assess the impact of the G431A,F433A mutations on binding partners of FAK, we isolated FAK protein complexes using immunoprecipitation and analyzed the interactomes using label-free mass spectrometry (Supplementary Fig. S1E–H). FAK-G431A,F433A exhibited impaired binding to all of the proteins for which binding to the more classical kinase-inactivating FAK-KD mutant was reduced (Fig. 1H and I; Supplementary Table S1). In addition, the FAK-G431A,F433A mutant protein interactome did not contain protein interactors that were also disrupted by the ATP-competitive FAK kinase inhibitor VS-4718, most notably Cdc37 and Wdr6 (Fig. 1H and I; Supplementary Table S1), when compared to FAK-KD, further supporting the notion that FAK-G431A,F433A both behaves like the more commonly used catalytically-inactive FAK-KD mutant and therefore better represents the actions of pharmacologically inhibited FAK-WT protein in terms of its interactome.

Identifying synergistic combinations with FAK inhibitors

A number of FAK inhibitors are currently undergoing clinical development (1). However, it is evident from studies to date that FAK inhibitors have limited effects on cancer cell growth and survival when used as a monotherapy. In contrast, FAK's role as a key signaling mediator of survival under conditions of cellular stress (34), including upon treatment of tumors with chemotherapy (9,35), suggests that targeting FAK in combination with other agents (that induce stress) may be required. To identify potential drug combination partners for FAK inhibitors, we performed a chemical-genetic, multiparametric, high-content phenotypic screen with a small-molecule compound library and compared phenotypic responses between SCC cell lines expressing FAK-G431A,F433A, FAK-WT, or no FAK (FAK−/−). These genetically matched SCC cells differed only with regard to FAK status and the resultant consequences of modulating FAK kinase activity on compound responses. The cells were incubated for 24 hours with an annotated compound library consisting of FDA-approved drugs and a mechanistic toolbox of kinase, epigenetic, and protease inhibitors to cover a range of biological areas (1280 and 176 compounds, respectively; Supplementary Table S2; compounds used at a final concentration of 10 μM). After compound treatment, the cells were fixed and labeled with Hoechst, phalloidin, and HCS CellMask to provide unbiased morphological profiling of the compound-induced phenotype. We measured multiple cellular features at the single-cell level to enable multiparametric analysis of compound-induced phenotypic responses, including principal component analysis to interrogate major phenotypic differences between compound effects across cell types that differ in FAK status (Fig. 2A).

We compared the SCC cells expressing FAK-G431A,F433A with cells expressing FAK-WT and compared FAK-deficient (−/−) cells with FAK-WT-expressing cells (Fig. 2A). Strikingly, the majority of compounds (69.2%; 9 compounds) whose phenotypes were influenced by FAK kinase activity were HDAC inhibitors (Fig. 2B). HDAC inhibitors induced morphological changes that required FAK kinase activity; representative images, while not conveying the multiple detailed readouts of the multiparametric phenotypic analysis performed, display visually obvious phenotypic differences following treatment with the HDAC inhibitor SAHA (trade name vorinostat, used hereafter), which is shown as an exemplar (Fig. 2C). In response to treatment with the HDAC inhibitor, FAK-WT-expressing SCC cells developed stress fiber-like F-actin structures and an enlarged cell area compared to untreated cells, which were not evident with the loss of either FAK or its kinase activity alone. Indeed, HDAC inhibitor treatment appeared to induce a distinct spindle cell morphology characterized by long thin cell protrusions in FAK−/− and FAK-G431A,F433A-expressing SCC cells relative to FAK-WT-expressing SCC cells (Fig. 2C). These data highlight the dependency of HDAC inhibitors on FAK signaling to induce strong phenotypic effects.

We next tested whether the morphological phenotypes observed following treatment with the HDAC inhibitor could be replicated in SCC cells expressing FAK-WT by co-treatment with small-molecule inhibitors of FAK and HDAC. We therefore selected vorinostat, the first HDAC inhibitor approved for clinical use, and panobinostat, a very potent HDAC inhibitor currently undergoing clinical trials (reviewed in (36)). Both vorinostat and panobinostat recapitulated the phenotypic response we observed using the FAK-G431A,F433A mutant (Supplementary Fig. S2A) when they were combined with the FAK inhibitor VS-4718, although this was not linked to a significant difference in cell proliferation in 2D cell culture when HDAC inhibitors were used to treat cells expressing the FAK-G431A,F433A mutant for 24 hours (Supplementary Fig. S2B). SCC cells expressing FAK-WT in the presence of the VS-4718 FAK inhibitor and treated with either HDAC inhibitor resulted in a weakly anti-proliferative effect after 72 hours of treatment (Supplementary Fig. S2C) and, in keeping with this, did not significantly alter the G1 cell cycle arrest induced by HDAC inhibitors in 2D culture (Supplementary Fig. S2D).

However, since we previously showed that FAK activity is required for proliferation of SCC cells in 3D culture, but not in 2D (6), we next tested whether the phenotypic effects observed were associated with an anti-proliferative combination in 3D culture. We found that combining FAK and HDAC inhibitors significantly and synergistically inhibited the growth and viability of spheroids composed of FAK-WT-expressing SCC cells, as quantified by measuring spheroid area and viability using calcein AM staining (Fig. 2D and E; Supplementary Fig. S2E–G), and resulted in a robust G1 cell cycle arrest (Fig. 2F and G). The inhibition of FAK and HDAC activity in SCC spheroids following 24 hours of compound treatment was assessed by measuring expression of phosphorylated FAK (pY397) and acetylated histone H3 (Fig. 2H). We assessed the effect of combining FAK and HDAC inhibitors on SCC tumors grown in CD-1 nude mice in vivo. We injected mice on both flanks with 2.5×10^5 SCC cells expressing FAK-WT and treated established tumors from day 0 with VS-4718 (75 mg/kg twice daily by oral gavage) and panobinostat (5 mg/kg, 5 out of 7 days by intraperitoneal injection), which as a combination was well tolerated as

we observed no significant change in mouse body weight over the course of the experiment (Supplementary Fig. S2H). We found that mice bearing SCC tumors expressing FAK-WT that were treated with a combination of VS-4718 and panobinostat exhibited significantly reduced tumor growth compared with either drug alone, each of which had a modest effect on tumor growth when used as a single agent (Fig. 2I).

Identification of cells that are sensitive to FAK and HDAC inhibitor combinations

To determine whether additional cancer cells (other than the SCC cells we had used for the chemical-genetic phenotypic screen) were sensitive to FAK and HDAC inhibitor combinations, we screened a panel of 33 commonly used human cell lines from a variety of cancer types. Cell lines were treated for 24 hours with FAK and HDAC inhibitor combinations before fixation and quantification of the number of Hoechst-labeled nuclei. We surveyed these cell lines for synergistic response to the combinations of FAK and HDAC inhibitors by quantifying the number of nuclei following 24 hours of drug treatment (Supplementary Fig. S3A and B), identifying a number of cell lines (5 out of 33 tested); two of these sensitive cell lines were examined further, namely A549 (lung adenocarcinoma) and Flo1 (esophageal adenocarcinoma) cells. These cell lines exhibited a strong reduction in proliferation in response to the combination of VS-4718 with HDAC inhibitors even in 2D culture (Fig. 3A). The ability of both A549 and Flo1 cells to grow in a colony formation assay over 7 days was visibly reduced by FAK and HDAC inhibitor combinations (Fig. 3B), and also when the cells were grown as spheroids (Supplementary Fig. S3C), when compared to either drug alone. These data confirmed that A549 and Flo1 cells were sensitive to the FAK and HDAC inhibitor combination, in 2D as well as 3D culture. In the case of these cells, the combination of the FAK inhibitor VS-4718 with either vorinostat or panobinostat synergistically reduced cell viability over a 3-day incubation period (Fig. 3C; Supplementary Fig. S4A–C) and significantly altered the cell cycle distribution, shifting cells into the G2/M phase, as quantified by DNA labeling with Hoechst (Fig. 3D). Apoptosis induced by each HDAC inhibitor in A549 and Flo1 cells was significantly increased by combining treatment with the FAK inhibitor VS-4718 (Fig. 3E). Importantly, the combination of FAK and HDAC inhibitors did not significantly attenuate the growth of human dermal fibroblasts as assessed by cell viability (Supplementary Fig. S4D). Finally, the growth of either A549 tumors in CD-1 nude mice or Flo1 tumors in NSG mice after subcutaneous injection was substantially impaired by combination treatment when compared to either treatment alone (Fig. 3F). These data show that, in a sub-set of cancer cell lines, treatment with a combination of FAK and HDAC inhibitors has synergistic and potent effects on tumor growth.

HDAC and FAK inhibitors together abolish FAK activation and promote nuclear exclusion of YAP

To understand the signaling events that occur in cells following treatment with the combination of FAK and HDAC inhibitors, we first assessed FAK-Y397 autophosphorylation. Although the FAK inhibitor VS-4718 was effective at partially inhibiting FAK's autophosphorylation (and presumed activation – a finding we have made previously in 2D culture (7)), treatment with either HDAC inhibitor also inhibited FAK-Y397 autophosphorylation to some extent by unknown mechanisms (Fig. 4A). When combined, VS-4718 together with either HDAC inhibitor significantly inhibited FAK-Y397

autophosphorylation to a greater (visibly complete) extent than either VS-4718 or HDAC inhibitor alone.

To examine downstream changes in signaling pathways following exposure of Flo1 cells to an effective dose-ratio combination of FAK and HDAC inhibitors relative to each monotherapy, we performed RPPA analysis across a number of canonical cancer cell signaling pathways. We found that YAP expression and phosphorylation were altered by the inhibitor combination (Supplementary Fig. S4E). YAP is a co-transcriptional regulator whose activity and nuclear localization are regulated by HDAC activity and FAK signaling (37,38). Therefore, we tested the effect of combined HDAC and FAK inhibitors on YAP. The FAK inhibitor VS-4718 induced YAP phosphorylation on residue S127, and HDAC inhibitors suppressed YAP protein expression, which was enhanced when the FAK and HDAC inhibitors were combined in both A549 and Flo1 cells (Fig. 4B). Furthermore, in both A549 and Flo1 cells, the FAK inhibitor significantly reduced nuclear localization of YAP, as judged by a reduction in YAP fluorescence intensity in the nucleus (Fig. 4C). Combining FAK and HDAC inhibitors reduced YAP nuclear localization to a greater extent than individual agents alone, as quantified by measurement of fluorescence intensity of anti-YAP cell labeling (Fig. 4D). Finally, we assessed the impact of combined FAK and HDAC inhibitor treatments on the expression of a YAP transcriptional target, Axl (39). We found that combination of FAK and HDAC inhibitors for 24 hours significantly reduced the expression of Axl in both A549 and Flo1 cell lines (Fig. 4E).

To determine whether YAP's localization was sensitive to the combination of FAK and HDAC inhibitors in cell lines in which synergistic anti-proliferative effects between FAK and HDAC inhibitors were not observed, we tested four combination-insensitive cancer cell lines. These did not display the same response with respect to YAP as the sensitive Flo1 or A549 cells, i.e. there was no significant anti-proliferative effects or any visible alteration of YAP nuclear localization in response to the combination of FAK and HDAC inhibitors (Supplementary Fig. S5A–C). Two of the non-responsive cell lines, SKGT4 and JH-Eso-AD1, displayed very little nuclear YAP, while the OAC-P4C and MFD1 cell lines displayed robust nuclear YAP localization that was not altered by the combination (Supplementary Fig. S5A). The combination of FAK and HDAC inhibitors in these four cell lines did not enhance anti-proliferative effects (as assessed by nuclear counts) or alter the nuclear localization of YAP, compared to DMSO treatment (Supplementary Fig. S5A–C), indicating that the latter is a strong correlate with combination sensitivity.

Finally, we examined the localization of YAP in vivo at the tumor margin (Fig. 5) as ECM contact is important for the activation of YAP (38,40). Here, we observed that YAP nuclear localization was reduced in tumors that were treated with the combination of the FAK inhibitor VS-4718 and the HDAC inhibitor panobinostat (Fig. 5A and B). Taken together, these data demonstrate that regulation of YAP correlates strongly with the morphological and synergistic anti-proliferative effects, and acts as a marker of cancer cells sensitive to the HDAC and FAK inhibitor combination.

Discussion

Here, we describe a completely novel and unbiased approach to identifying useful anti-cancer combinations of small-molecule inhibitors, which combines genetic modulation of cancer cells and high-content phenotypic screening to genetically fix one axis of combination screens. Using this strategy, we were able to capture phenotypic effects in 2D cell culture models that predicted anti-tumor growth in vivo. We discovered a novel combination of FAK and HDAC inhibitors that demonstrate synergistic effects in a cancer cell context-dependent manner. This is important because, while FAK is regarded as a high-value druggable target for cancer therapy, it is becoming evident that FAK inhibitors will best be used in combination as FAK is a key stress-induced survival pathway, including when cells are treated with anti-cancer therapies (2,5,9,41). In addition to HDAC inhibitors, which formed the predominant class of compounds that synergized with kinase-defective FAK, we identified a further 18 putative hits representing previously approved drugs that have not yet been studied further (Supplementary Table 2). These data imply that there are likely to be a number of useful co-vulnerabilities in cancer cells in which FAK mediates critical survival signaling. Because the FAK and HDAC inhibitor combination was effective in a sub-set of cancer cells, defined by co-promoted changes in the phosphorylation and nuclear localization of the transcriptional co-activator YAP, it will be important to continue to identify additional collaborating targets and inhibitors that are synergistic with FAK inhibitors.

Regarding the value of the multiparametric phenotypic screening approach, we noted that the strongest FAK-dependent cell phenotypes following compound screening in 2D culture of SCC cells were not related to proliferation, but rather changes in morphometric phenotypes; SCC cells exhibit a mesenchymal-like morphology that, upon HDAC inhibitor treatment, resulted in enlargement of cell area and an increase in the number of F-actin stress fibers (Fig. 2C). FAK is a critical regulator of focal adhesions that links cellular attachment to the extracellular matrix to the actin cytoskeleton, providing adhesion-mediated survival signals (34,42). HDAC6 is cytoplasmic and has also been reported to regulate the dynamics of adhesions and cell spreading (43). Since vorinostat and panobinostat are broad-spectrum HDAC inhibitors, the FAK-dependent morphological changes we observe in SCC cells could operate through HDAC6 inhibition. We predict that the morphological changes following HDAC inhibitor treatment were indicative of cellular stress and that FAK kinase activity could mitigate against a stress response, thus providing a vulnerability that could be exploited using a the FAK/HDAC inhibitor drug combination. We have also shown that the morphometric phenotypes predicted a combination that inhibited tumor growth in mice. More traditional screening strategies generally employ single endpoint analysis, such as cytotoxic screens, where cell viability, or number, in 2D cultures. We have, here and previously (6), shown that FAK inhibition (either genetic or pharmacological) in SCC cells does not inhibit proliferation or viability in 2D, but does so in 3D and in vivo. In the work presented here, prior knowledge of FAK biology in SCC cells (6) led us to predict that a phenotypic dependency on FAK kinase activity in 2D would prove to be an effective anti-proliferative combination in 3D assays and, potentially, in vivo, demonstrating the power of capturing an unbiased complete description of a compound's

morphometric effects. The wealth of information, and predictive value, contained in the cellular morphological fingerprints following perturbation has been well recognized, and their quantification is increasingly being used as an unbiased method to profile compounds through multiparametric high-content microscopy, coupled to new emerging image-informatics and machine learning solutions (18–20,44–46).

Regarding use of mutation of residues G431 and F433 of the glycine-rich loop in the FAK kinase domain, these are conservative substitutions that are not expected to affect the structure of the kinase domain as this loop is a highly mobile and unstructured part of the kinase domain (47). Hsp90 and its co-chaperone Cdc37 interact with approximately 60% of the mammalian kinome (12), and so fixing one axis of a combination screen could provide a genetic and specific means to test the target validity of a particular kinase (rather than relying on the selectivity of a given compound), enabling targeting of kinases that do not currently have specific kinase inhibitors and reduces the off-target effects of polypharmacology in screens. Thus, the novel chemical-genetic phenotypic screening approach we describe here may represent a broader strategy for rapidly identifying novel kinase inhibitor combinations.

HDACs are a widely studied class of epigenetic regulators that are frequently dysregulated in cancer and so have long been targets of therapeutic research (36). There are currently 169 recruiting or active clinical trials using HDAC inhibitors (ClinicalTrials.gov; 31 involving panobinostat and 63 involving vorinostat), the majority of which are in combination with other agents (reviewed in (48)). The overall strategy of targeting HDACs for cancer therapy is to revert “cancerous” epigenetic changes towards a more “normal”-like cell state and to achieve the reactivation of tumor suppressor pathways, growth arrest, and apoptosis or cell death. These changes undoubtedly will cause cancer cells stress, and it may be that FAK is a key component of the pathways that mitigate against stress responses and cancer cell death. We note that cell shape (which FAK regulates via well-documented effects on actin and adhesion networks) can alter histone acetylation (49) and that gene expression profiling of HDAC inhibitor resistance in human myeloma cell lines identified actin cytoskeleton-associated genes, and FAK itself, as part of a resistance gene signature (50). This supports the link that we have identified here between the likely regulation of the cellular epigenetic state by HDAC activity and FAK activity, revealing a co-dependency in multiple cancer cell lines.

Mechanistically, we have found that the combination of FAK and HDAC inhibitors results in complete abolition of FAK kinase activity, more so than the partial suppression of FAK kinase activity that is achieved with a FAK inhibitor alone, suggesting that residual adhesion signaling via FAK is performing a critical survival role in these cells. Since there is no apparent reason why HDAC inhibitors would act directly upon FAK kinase function – indeed, shorter periods of incubation with HDAC inhibitors do not affect FAK autophosphorylation (Fig. 4B) – we postulate that the effects of HDAC inhibitors are likely indirect, perhaps by regulating expression of gene products that influence FAK’s kinase activity.

YAP and TAZ are transcriptional activators that regulate many cell responses by transducing mechanical, polarity, and growth factor signaling into a transcriptional response (51). YAP and TAZ activation correlates with grade, metastasis, and poor outcome in breast, lung, liver, pancreatic, and skin cancer (reviewed in (52)), and activation of YAP leads to drug resistance, for example, by increased cytoskeletal tension and/or ECM deposition from cancer-associated fibroblasts in melanoma cells (9,37,53–55). HDAC inhibitors reduce YAP expression in cancer cells (56,57), and FAK, and other focal adhesion proteins, are reported to regulate YAP phosphorylation by LATS1/2 kinase on S127, so preventing its nuclear translocation (37). In our studies, the combination of FAK and HDAC inhibitors collaboratively reinforced the inhibition of YAP activity; firstly, HDAC inhibition reduced YAP expression, and secondly, FAK inhibition impaired the nuclear translocation, and hence transcriptional activity, of YAP. Interestingly, FAK is implicated in an integrin α3-FAK signaling axis that drives YAP nuclear localization and proliferation of incisor stem cells (40); this pathway could be active in some tumor cells to regulate the proliferation of putative cancer stem cell-like populations, as is reported in triple-negative breast cancer (58). The FAK inhibitor used in our study, VS-4718, has been de-prioritized by Verastem and withdrawn from clinical development (ClinicalTrials.gov identifier NCT02651727); however, other FAK inhibitors (VS-6063 and GSK2256098) and various HDAC inhibitors are currently under clinical development independently in several cancer types (36,42), and therefore the combination we have identified can be taken forward for clinical testing as a putative combination therapy.

Supplementary Material

Refer to Web version on PubMed Central for supplementary material.

Acknowledgments

We thank R. Pilkington for assistance with mass spectrometry, K. G. Macleod for RPPA analysis, T. R. Hupp for providing esophageal cancer cells, and V. G. Brunton for advice with animal experiments.

Financial Support

This work was supported by Cancer Research UK Program Grants (C157/A15703 and C157/A24837) and a European Research Council Advanced Investigator Grant (294440 Cancer Innovation) to M. C. Frame.

References

1. Lee BY, Timpson P, Horvath LG, Daly RJ. FAK signaling in human cancer as a target for therapeutics. Pharmacol Ther. 2015; 146 :132–49. DOI: 10.1016/j.pharmthera.2014.10.001 [PubMed: 25316657]
2. Serrels A, Lund T, Serrels B, Byron A, McPherson RC, von Kriegsheim A, et al. Nuclear FAK controls chemokine transcription, Tregs, and evasion of anti-tumor immunity. Cell. 2015; 163 (1) :160–73. DOI: 10.1016/j.cell.2015.09.001 [PubMed: 26406376]
3. Canel M, Byron A, Sims AH, Cartier J, Patel H, Frame MC, et al. Nuclear FAK and Runx1 Cooperate to Regulate IGFBP3, Cell-Cycle Progression, and Tumor Growth. Cancer Res. 2017; 77 (19) :5301–12. DOI: 10.1158/0008-5472.CAN-17-0418 [PubMed: 28807942]
4. Lim ST, Chen XL, Lim Y, Hanson DA, Vo TT, Howerton K, et al. Nuclear FAK promotes cell proliferation and survival through FERM-enhanced p53 degradation. Mol Cell. 2008; 29 (1) :9–22. DOI: 10.1016/j.molcel.2007.11.031 [PubMed: 18206965]

5. Sandilands E, Serrels B, McEwan DG, Morton JP, Macagno JP, McLeod K, et al. Autophagic targeting of Src promotes cancer cell survival following reduced FAK signalling. Nat Cell Biol. 2011; 14 (1) :51–60. DOI: 10.1038/ncb2386 [PubMed: 22138575]
6. Serrels A, McLeod K, Canel M, Kinnaird A, Graham K, Frame MC, et al. The role of focal adhesion kinase catalytic activity on the proliferation and migration of squamous cell carcinoma cells. Int J Cancer. 2012; 131 (2) :287–97. DOI: 10.1002/ijc.26351 [PubMed: 21823119]
7. Serrels B, McGivern N, Canel M, Byron A, Johnson SC, McSorley HJ, et al. IL-33 and ST2 mediate FAK-dependent antitumor immune evasion through transcriptional networks. Sci Signal. 2017; 10 (508) doi: 10.1126/scisignal.aan8355
8. Serrels B, Sandilands E, Serrels A, Baillie G, Houslay MD, Brunton VG, et al. A complex between FAK, RACK1, and PDE4D5 controls spreading initiation and cancer cell polarity. Curr Biol. 2010; 20 (12) :1086–92. DOI: 10.1016/j.cub.2010.04.042 [PubMed: 20493699]
9. Hirata E, Girotti MR, Viros A, Hooper S, Spencer-Dene B, Matsuda M, et al. Intravital imaging reveals how BRAF inhibition generates drug-tolerant microenvironments with high integrin beta1/FAK signaling. Cancer Cell. 2015; 27 (4) :574–88. DOI: 10.1016/j.ccell.2015.03.008 [PubMed: 25873177]
10. Jones SF, Siu LL, Bendell JC, Cleary JM, Razak AR, Infante JR, et al. A phase I study of VS-6063, a second-generation focal adhesion kinase inhibitor, in patients with advanced solid tumors. Invest New Drugs. 2015; 33 (5) :1100–7. DOI: 10.1007/s10637-015-0282-y [PubMed: 26334219]
11. Soria JC, Gan HK, Blagden SP, Plummer R, Arkenau HT, Ranson M, et al. A phase I, pharmacokinetic and pharmacodynamic study of GSK2256098, a focal adhesion kinase inhibitor, in patients with advanced solid tumors. Ann Oncol. 2016; 27 (12) :2268–74. DOI: 10.1093/annonc/mdw427 [PubMed: 27733373]
12. Taipale M, Krykbaeva I, Koeva M, Kayatekin C, Westover KD, Karras GI, et al. Quantitative analysis of HSP90-client interactions reveals principles of substrate recognition. Cell. 2012; 150 (5) :987–1001. DOI: 10.1016/j.cell.2012.06.047 [PubMed: 22939624]
13. Workman P, Burrows F, Neckers L, Rosen N. Drugging the cancer chaperone HSP90: combinatorial therapeutic exploitation of oncogene addiction and tumor stress. Ann N Y Acad Sci. 2007; 1113 :202–16. DOI: 10.1196/annals.1391.012 [PubMed: 17513464]
14. Polier S, Samant RS, Clarke PA, Workman P, Prodromou C, Pearl LH. ATP-competitive inhibitors block protein kinase recruitment to the Hsp90-Cdc37 system. Nature chemical biology. 2013; 9 (5) :307–12. DOI: 10.1038/nchembio.1212 [PubMed: 23502424]
15. Terasawa K, Minami Y. A client-binding site of Cdc37. FEBS J. 2005; 272 (18) :4684–90. DOI: 10.1111/j.1742-4658.2005.04884.x [PubMed: 16156789]
16. Terasawa K, Yoshimatsu K, Iemura S, Natsume T, Tanaka K, Minami Y. Cdc37 interacts with the glycine-rich loop of Hsp90 client kinases. Mol Cell Biol. 2006; 26 (9) :3378–89. DOI: 10.1128/MCB.26.9.3378-3389.2006 [PubMed: 16611982]
17. Reisen F, Sauty de Chalon A, Pfeifer M, Zhang X, Gabriel D, Selzer P. Linking phenotypes and modes of action through high-content screen fingerprints. Assay Drug Dev Technol. 2015; 13 (7) :415–27. DOI: 10.1089/adt.2015.656 [PubMed: 26258308]
18. Caie PD, Walls RE, Ingleston-Orme A, Daya S, Houslay T, Eagle R, et al. High-content phenotypic profiling of drug response signatures across distinct cancer cells. Mol Cancer Ther. 2010; 9 (6) :1913–26. DOI: 10.1158/1535-7163.MCT-09-1148 [PubMed: 20530715]
19. Ljosa V, Caie PD, Horst R, Ter Sokolnicki KL, Jenkins EL, Daya S, et al. Comparison of methods for image-based profiling of cellular morphological responses to small-molecule treatment. J Biomol Screen. 2013; 18 (10) :1321–9. DOI: 10.1177/1087057113503553 [PubMed: 24045582]
20. Warchal SJ, Dawson JC, Carragher NO. Development of the Theta Comparative Cell Scoring Method to Quantify Diverse Phenotypic Responses Between Distinct Cell Types. Assay Drug Dev Technol. 2016; 14 (7) :395–406. DOI: 10.1089/adt.2016.730 [PubMed: 27552144]
21. Warchal SJ, Unciti-Broceta A, Carragher NO. Next-generation phenotypic screening. Future Med Chem. 2016; 8 (11) :1331–47. DOI: 10.4155/fmc-2016-0025 [PubMed: 27357617]
22. Horvath P, Aulner N, Bickle M, Davies AM, Nery ED, Ebner D, et al. Screening out irrelevant cell-based models of disease. Nat Rev Drug Discov. 2016; 15 (11) :751–69. DOI: 10.1038/nrd.2016.175 [PubMed: 27616293]

23. Hildebrand JD, Schaller MD, Parsons JT. Identification of sequences required for the efficient localization of the focal adhesion kinase, pp125FAK, to cellular focal adhesions. J Cell Biol. 1993; 123 (4) :993–1005. [PubMed: 8227154]
24. McLean GW, Komiyama NH, Serrels B, Asano H, Reynolds L, Conti F, et al. Specific deletion of focal adhesion kinase suppresses tumor formation and blocks malignant progression. Genes Dev. 2004; 18 (24) :2998–3003. DOI: 10.1101/gad.316304 [PubMed: 15601818]
25. Macleod KG, Serrels B, Carragher NO. Reverse Phase Protein Arrays and Drug Discovery. Methods Mol Biol. 2017; 1647 :153–69. DOI: 10.1007/978-1-4939-7201-2_10 [PubMed: 28809001]
26. McQuin C, Goodman A, Chernyshev V, Kamentsky L, Cimini BA, Karhohs KW, et al. CellProfiler 3.0: Next-generation image processing for biology. PLoS Biol. 2018; 16 (7) e2005970 doi: 10.1371/journal.pbio.2005970 [PubMed: 29969450]
27. Bankhead P, Loughrey MB, Fernandez JA, Dombrowski Y, McArt DG, Dunne PD, et al. QuPath: Open source software for digital pathology image analysis. Sci Rep. 2017; 7 (1) 16878 doi: 10.1038/s41598-017-17204-5 [PubMed: 29203879]
28. Ianevski A, He L, Aittokallio T, Tang J. SynergyFinder: a web application for analyzing drug combination dose-response matrix data. Bioinformatics. 2017; 33 (15) :2413–5. DOI: 10.1093/bioinformatics/btx162 [PubMed: 28379339]
29. Turriziani B, Garcia-Munoz A, Pilkington R, Raso C, Kolch W, von Kriegsheim A. On-beads digestion in conjunction with data-dependent mass spectrometry: a shortcut to quantitative and dynamic interaction proteomics. Biology (Basel). 2014; 3 (2) :320–32. DOI: 10.3390/biology3020320 [PubMed: 24833512]
30. Cox J, Mann M. MaxQuant enables high peptide identification rates, individualized p.p.b.-range mass accuracies and proteome-wide protein quantification. Nat Biotechnol. 2008; 26 (12) :1367–72. DOI: 10.1038/nbt.1511 [PubMed: 19029910]
31. Tyanova S, Temu T, Sinitcyn P, Carlson A, Hein MY, Geiger T, et al. The Perseus computational platform for comprehensive analysis of (prote)omics data. Nat Methods. 2016; 13 (9) :731–40. DOI: 10.1038/nmeth.3901 [PubMed: 27348712]
32. Shevchenko A, Wilm M, Vorm O, Mann M. Mass spectrometric sequencing of proteins silver-stained polyacrylamide gels. Anal Chem. 1996; 68 (5) :850–8. [PubMed: 8779443]
33. Farrell J, Kelly C, Rauch J, Kida K, Garcia-Munoz A, Monsefi N, et al. HGF induces epithelial-to-mesenchymal transition by modulating the mammalian hippo/MST2 and ISG15 pathways. J Proteome Res. 2014; 13 (6) :2874–86. DOI: 10.1021/pr5000285 [PubMed: 24766643]
34. Frisch SM, Vuori K, Ruoslahti E, Chan-Hui PY. Control of adhesion-dependent cell survival by focal adhesion kinase. J Cell Biol. 1996; 134 (3) :793–9. [PubMed: 8707856]
35. Frame MC, Serrels A. FAK to the rescue: activated stroma promotes a “safe haven” for BRAF-mutant melanoma cells by inducing FAK signaling. Cancer Cell. 2015; 27 (4) :429–31. DOI: 10.1016/j.ccell.2015.03.013 [PubMed: 25873166]
36. Li Y, Seto E. HDACs and HDAC Inhibitors in Cancer Development and Therapy. Cold Spring Harb Perspect Med. 2016; 6 (10) doi: 10.1101/cshperspect.a026831
37. Kim NG, Gumbiner BM. Adhesion to fibronectin regulates Hippo signaling via the FAK-Src-PI3K pathway. J Cell Biol. 2015; 210 (3) :503–15. DOI: 10.1083/jcb.201501025 [PubMed: 26216901]
38. Elbediwy A, Vincent-Mistiaen ZI, Spencer-Dene B, Stone RK, Boeing S, Wculek SK, et al. Integrin signalling regulates YAP and TAZ to control skin homeostasis. Development. 2016; 143 (10) :1674–87. DOI: 10.1242/dev.133728 [PubMed: 26989177]
39. Cui ZL, Han FF, Peng XH, Chen X, Luan CY, Han RC, et al. YES-associated protein 1 promotes adenocarcinoma growth and metastasis through activation of the receptor tyrosine kinase Axl. Int J Immunopathol Pharmacol. 2012; 25 (4) :989–1001. DOI: 10.1177/039463201202500416 [PubMed: 23298489]
40. Hu JK, Du W, Shelton SJ, Oldham MC, DiPersio CM, Klein OD. An FAK-YAP-mTOR Signaling Axis Regulates Stem Cell-Based Tissue Renewal in Mice. Cell Stem Cell. 2017; 21 (1) :91–106. e6 doi: 10.1016/j.stem.2017.03.023 [PubMed: 28457749]

41. Storch K, Sagerer A, Cordes N. Cytotoxic and radiosensitizing effects of FAK targeting in human glioblastoma cells in vitro. Oncol Rep. 2015; 33 (4) :2009–16. DOI: 10.3892/or.2015.3753 [PubMed: 25625667]
42. Golubovskaya VM. Targeting FAK in human cancer: from finding to first clinical trials. Front Biosci (Landmark Ed). 2014; 19 :687–706. [PubMed: 24389213]
43. Tran AD, Marmo TP, Salam AA, Che S, Finkelstein E, Kabarriti R, et al. HDAC6 deacetylation of tubulin modulates dynamics of cellular adhesions. J Cell Sci. 2007; 120 (Pt 8) :1469–79. DOI: 10.1242/jcs.03431 [PubMed: 17389687]
44. Caicedo JC, Cooper S, Heigwer F, Warchal S, Qiu P, Molnar C, et al. Data-analysis strategies for image-based cell profiling. Nat Methods. 2017; 14 (9) :849–63. DOI: 10.1038/nmeth.4397 [PubMed: 28858338]
45. Bray MA, Gustafsdottir SM, Rohban MH, Singh S, Ljosa V, Sokolnicki KL, et al. A dataset of images and morphological profiles of 30 000 small-molecule treatments using the Cell Painting assay. Gigascience. 2017; 6 (12) :1–5. DOI: 10.1093/gigascience/giw014
46. Bray MA, Singh S, Han H, Davis CT, Borgeson B, Hartland C, et al. Cell Painting, a high-content image-based assay for morphological profiling using multiplexed fluorescent dyes. Nature protocols. 2016; 11 (9) :1757–74. DOI: 10.1038/nprot.2016.105 [PubMed: 27560178]
47. Lietha D, Cai X, Ceccarelli DF, Li Y, Schaller MD, Eck MJ. Structural basis for the autoinhibition of focal adhesion kinase. Cell. 2007; 129 (6) :1177–87. DOI: 10.1016/j.cell.2007.05.041 [PubMed: 17574028]
48. Suraweera A, O'Byrne KJ, Richard DJ. Combination Therapy With Histone Deacetylase Inhibitors (HDACi) for the Treatment of Cancer: Achieving the Full Therapeutic Potential of HDACi. Front Oncol. 2018; 8 :92. doi: 10.3389/fonc.2018.00092 [PubMed: 29651407]
49. Le Beyec J, Xu R, Lee SY, Nelson CM, Rizki A, Alcaraz J, et al. Cell shape regulates global histone acetylation in human mammary epithelial cells. Exp Cell Res. 2007; 313 (14) :3066–75. DOI: 10.1016/j.yexcr.2007.04.022 [PubMed: 17524393]
50. Mithraprabhu S, Khong T, Spencer A. Overcoming inherent resistance to histone deacetylase inhibitors in multiple myeloma cells by targeting pathways integral to the actin cytoskeleton. Cell Death Dis. 2014; 5 e1134 doi: 10.1038/cddis.2014.98 [PubMed: 24651437]
51. Zanconato F, Cordenonsi M, Piccolo S. YAP and TAZ: a signalling hub of the tumour microenvironment. Nat Rev Cancer. 2019; 19 (8) :454–64. DOI: 10.1038/s41568-019-0168-y [PubMed: 31270418]
52. Zanconato F, Cordenonsi M, Piccolo S. YAP/TAZ at the Roots of Cancer. Cancer Cell. 2016; 29 (6) :783–803. DOI: 10.1016/j.ccell.2016.05.005 [PubMed: 27300434]
53. Calvo F, Ege N, Grande-Garcia A, Hooper S, Jenkins RP, Chaudhry SI, et al. Mechanotransduction and YAP-dependent matrix remodelling is required for the generation and maintenance of cancer-associated fibroblasts. Nat Cell Biol. 2013; 15 (6) :637–46. DOI: 10.1038/ncb2756 [PubMed: 23708000]
54. Elosegui-Artola A, Andreu I, Beedle AEM, Lezamiz A, Uroz M, Kosmalska AJ, et al. Force Triggers YAP Nuclear Entry by Regulating Transport across Nuclear Pores. Cell. 2017; 171 (6) :1397–410. e14 doi: 10.1016/j.cell.2017.10.008 [PubMed: 29107331]
55. Lin L, Sabnis AJ, Chan E, Olivas V, Cade L, Pazarentzos E, et al. The Hippo effector YAP promotes resistance to RAF- and MEK-targeted cancer therapies. Nat Genet. 2015; 47 (3) :250–6. DOI: 10.1038/ng.3218 [PubMed: 25665005]
56. Han H, Yang B, Nakaoka HJ, Yang J, Zhao Y, Le Nguyen K, et al. Hippo signaling dysfunction induces cancer cell addiction to YAP. Oncogene. 2018; 37 (50) :6414–24. DOI: 10.1038/s41388-018-0419-5 [PubMed: 30068939]
57. Heinemann A, Cullinane C, De Paoli-Iseppi R, Wilmott JS, Gunatilake D, Madore J, et al. Combining BET and HDAC inhibitors synergistically induces apoptosis of melanoma and suppresses AKT and YAP signaling. Oncotarget. 2015; 6 (25) :21507–21. DOI: 10.18632/oncotarget.4242 [PubMed: 26087189]
58. Kolev VN, Tam WF, Wright QG, McDermott SP, Vidal CM, Shapiro IM, et al. Inhibition of FAK kinase activity preferentially targets cancer stem cells. Oncotarget. 2017; 8 (31) :51733–47. DOI: 10.18632/oncotarget.18517 [PubMed: 28881682]

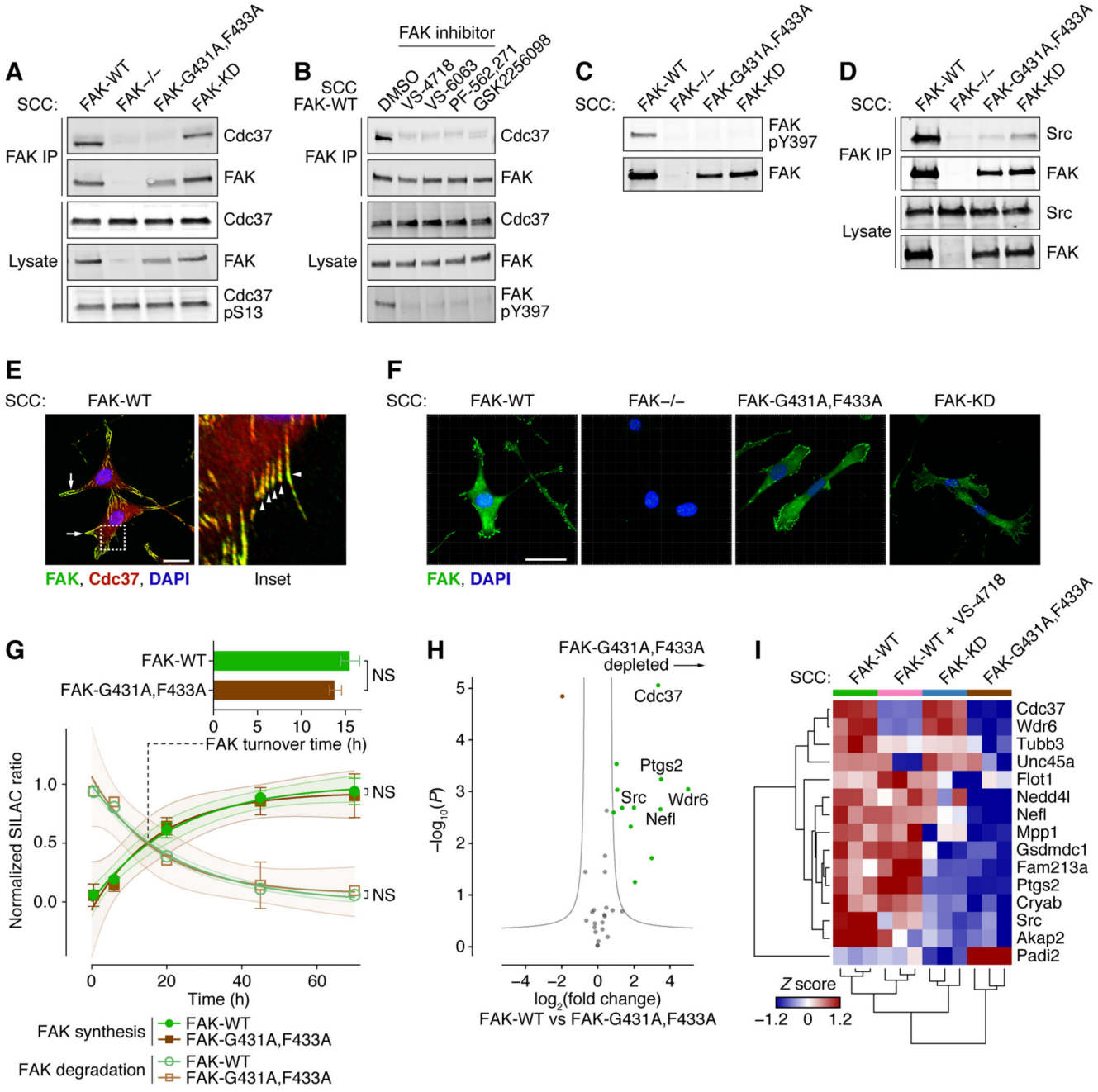

Figure 1. Disruption of Cdc37 chaperone binding to FAK mimics FAK kinase inhibition.

A, IP of FAK from SCC FAK-WT, FAK−/−, FAK-G431A,F433A, and FAK-KD cell lysates, immunoblotted for FAK, Cdc37, and phosphorylated Cdc37 (S13). **B**, IP of FAK from SCC FAK-WT cells treated with DMSO (0.1%) or 250 nM VS-4718, VS-6063, PF-562,271, or GSK2256098 for 24 h, immunoblotted for FAK, phosphorylated FAK (Y397), and Cdc37. **C**, Lysates from SCC FAK-WT, FAK−/−, FAK-G431A,F433A, and FAK-KD cells, immunoblotted for FAK and phosphorylated FAK (Y397). **D**, IP of FAK from SCC FAK-WT, FAK−/−, FAK-G431A,F433A, and FAK-KD cell lysates, immunoblotted for FAK and

Src. **E**, SCC FAK-WT cells seeded on glass coverslips, fixed, and labeled with anti-FAK (green), anti-Cdc37 (red), and DAPI (blue). Inset (right) represents dashed boxed region of main image. Arrows and arrowheads (inset) indicate examples of regions of colocalization of FAK and Cdc37. Scale bar, 20 μm. **F**, SCC FAK-WT, FAK−/−, FAK-G431A,F433A, and FAK-KD cells seeded on glass coverslips, fixed, and labeled with anti-FAK (green) and DAPI (blue). Scale bars, 20 μm. **G**, FAK synthesis and degradation profiles quantified by metabolic labeling and mass spectrometry. FAK-WT (green) and FAK-G431A,F433A (brown) synthesis and degradation curves were determined from normalized SILAC ratio profiles by nonlinear regression and plotted as means ± SEM with best fit curves and 95% confidence interval bands ($n \geq 5$ peptides; representative of three independent experiments). NS, not significant (extra sum-of-squares F test). Bar chart inset summarizes inferred 50% protein turnover times for FAK-WT and FAK-G431A,F433A, plotted as means ± SD ($n = 3$ independent experiments). NS, not significant (two-tailed Mann–Whitney U test). **H**, Label-free mass spectrometric characterization of FAK-interacting proteins isolated by IP of FAK from SCC FAK-WT and FAK-G431A,F433A cell lysates. Specific FAK-binding proteins were determined versus IP from SCC FAK−/− cells ($n = 3$ independent experiments), satisfying $Q < 0.05$ (Student's t-test with permutation-based FDR correction). Gray curves show the threshold for significant differential regulation (FDR, 5%; artificial within-groups variance, 1). Proteins satisfying $P < 0.01$ and fold change > 4 are labeled with gene names for clarity. **I**, Label-free mass spectrometric characterization of FAK-interacting proteins isolated by IP from SCC FAK-WT, FAK-KD, and FAK-G431A,F433A cell lysates and lysates from SCC FAK-WT cells treated with 250 nM VS-4718 ($n = 3$ independent experiments). Normalized label-free quantification of protein abundance for each protein was converted to a Z score. Differentially regulated, specific FAK-binding proteins satisfying $Q < 0.05$ (one-way ANOVA with permutation-based FDR correction) were hierarchically clustered and displayed as a heatmap. Proteins are labeled with gene names for clarity.

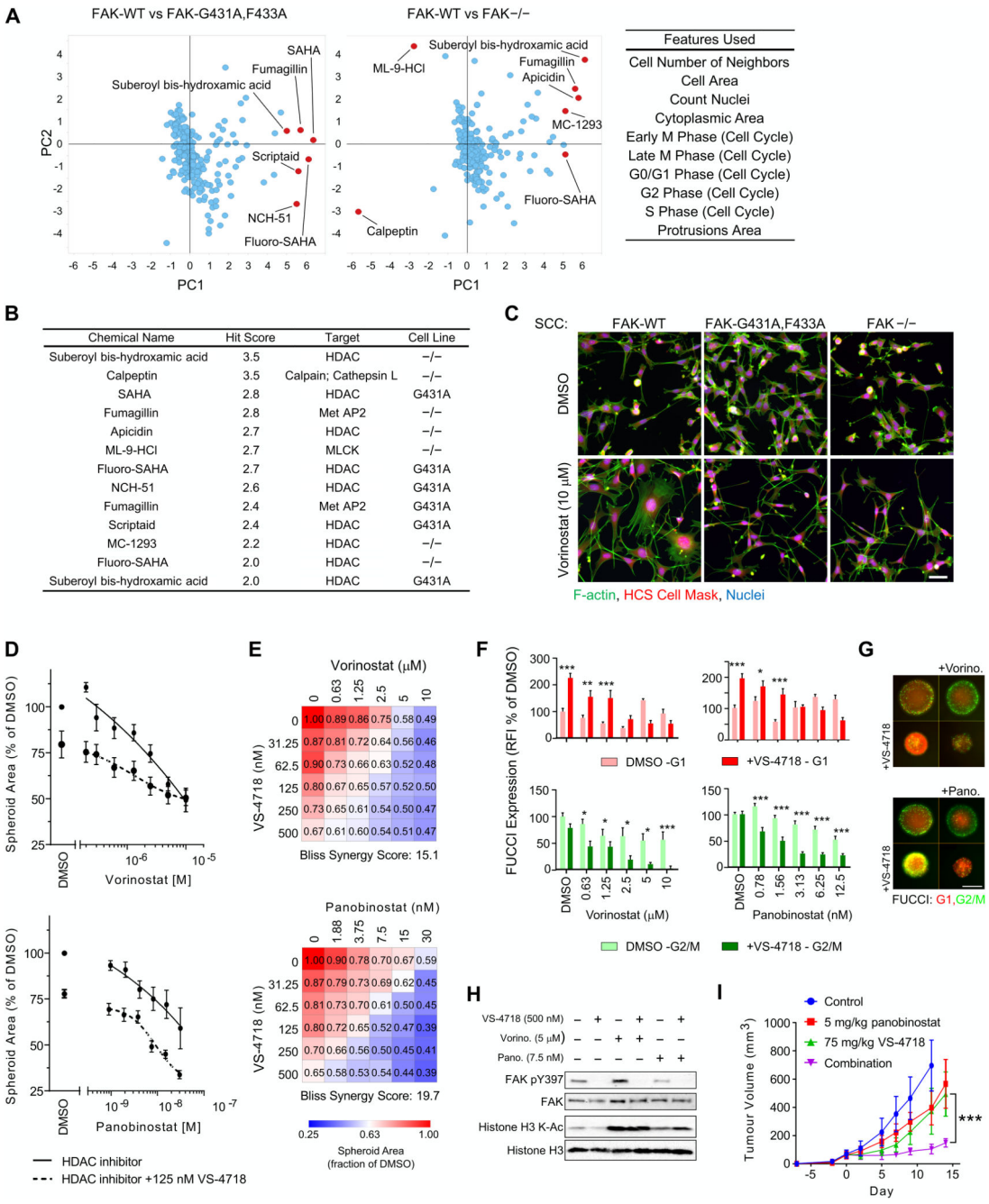

Chemical Name	Hit Score	Target	Cell Line
Suberoyl bis-hydroxamic acid	3.5	HDAC	−/−
Calpeptin	3.5	Calpain; Cathepsin L	−/−
SAHA	2.8	HDAC	G431A
Fumagillin	2.8	Met AP2	−/−
Apicidin	2.7	HDAC	−/−
ML-9-HCl	2.7	MLCK	−/−
Fluoro-SAHA	2.7	HDAC	G431A
NCH-51	2.6	HDAC	G431A
Fumagillin	2.4	Met AP2	G431A
Scriptaid	2.4	HDAC	G431A
MC-1293	2.2	HDAC	−/−
Fluoro-SAHA	2.0	HDAC	−/−
Suberoyl bis-hydroxamic acid	2.0	HDAC	G431A

Figure 2. Identification of synergistic combinations with FAK kinase inhibitors.

A, Summary of compound screen to identify drug sensitivity in the presence of reduced FAK kinase activity. To identify differential phenotypic effects between FAK-WT and FAK-mutant (FAK-G431A,F433A or FAK−/−) cells, for each image-based measurement *Z*-score, the FAK-WT value was subtracted from each FAK mutant value. Differential phenotypic effects were analyzed by principal component analysis. Principal components (PCs) 1 and 2 account for 51.3% and 22.1% of the total variance, respectively. Cellular features used in the phenotypic analysis are listed in the inset (right). **B**, Hit compounds identified in

the phenotypic screen. Vorinostat is labeled as SAHA in **A** and **B**. **C**, SCC FAK-WT, FAK-G431A,F433A, and FAK−/− cells treated with 10 μM vorinostat. Blue, nuclei; green, F-actin; red, HCS Cell Mask. Scale bar, 50 μm. **D**, Combination of vorinostat (top) or panobinostat (bottom) with VS-4718 inhibits spheroid growth. **E**, Dose matrices of spheroid area following treatment with vorinostat (top) or panobinostat (bottom) in combination with VS-4178 for 7 days. **F**, Quantification of RFP (G1 phase; top) and GFP (G2/M phase; bottom) FUCCI cell cycle reporter expression in SCC FAK-WT spheroids treated with vorinostat (left) or panobinostat (right) for 7 days. For combination treatments with VS-4718, 500 nM VS-4718 was used. RFI, relative fluorescence intensity. **G**, SCC FAK-WT spheroids expressing FUCCI cell cycle reporter were treated for 7 days with vorinostat (Vorino.; 1.25 μM) or panobinostat (Pano.; 6.25 nM) in combination with VS-4718 (500 nM). For **D**, **E**, and **F**, data are normalized to DMSO values and are displayed as means ± SEM ($n = 3$ independent experiments). *, $P < 0.05$; **, $P < 0.01$; ***, $P < 0.001$ (two-way ANOVA). **H**, Lysates from SCC FAK-WT spheroids treated with VS-4718, vorinostat (Vorino.), or panobinostat (Pano.) for 24 hours and immunoblotted for FAK, phosphorylated FAK (Y397), histone H3, and acetylated (K-Ac) histone H3. **I**, Combination of panobinostat and VS-4718 inhibits SCC FAK-WT tumor growth. Mice were treated with drug(s) from day 0. Group tumor volumes are displayed as mean ± SEM [$n = 5$ mice per group (2 tumors per mouse)]. ***, $P < 0.001$ (one-way ANOVA).

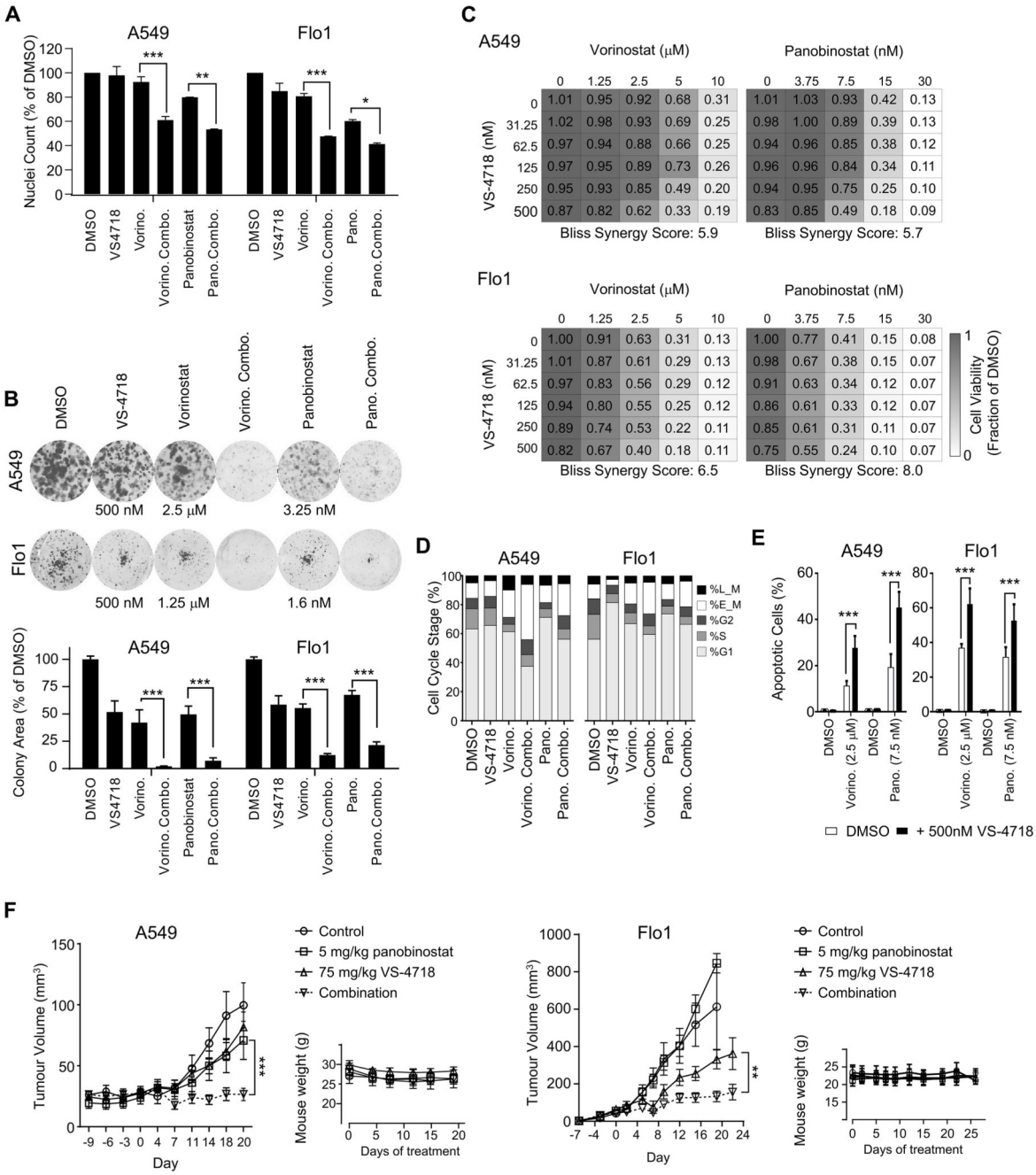

Figure 3. Identification of cells that are sensitive to FAK and HDAC inhibitor combinations.

A, Nuclei counts of A549 (left) and Flo1 (right) cells following treatment with vorinostat (5 μM), panobinostat (7.5 nM), and VS-4718 (500 nM) for 24 hours. Data are normalized to DMSO values and are displayed as mean ± SEM ($n = 2$ independent experiments). *, $P < 0.05$; **, $P < 0.01$; ***, $P < 0.001$ (two-way ANOVA). **B**, Combined inhibition of FAK and HDAC blocks colony formation. Representative images are shown (top). Bar charts (bottom) are plotted as means ± SEM ($n \geq 3$ independent experiments). **C**, Combination of FAK and HDAC inhibition reduces cell viability. Dose matrices of viability of A549 (top)

and Flo1 (bottom) cells following treatment with vorinostat (μM; left) or panobinostat (nM; right). **D**, Cell cycle distribution in A549 (left) and Flo1 (right) cells following treatment with the same drugs as used in **B** for 24 hours. Results in **C** and **D** are displayed as means ($n \geq 3$ independent experiments). **E**, FAK and HDAC inhibition enhances the induction of apoptosis in A549 (left) and Flo1 (right) cells. Bar charts are plotted as means ± SEM ($n \geq 3$ independent experiments). **F**, Combination of panobinostat and VS-4718 inhibits A549 (left) or Flo1 (right) tumor growth. Tumor volumes are plotted as means ± SEM [$n \geq 4$ mice per group (2 tumors per mouse)]. Mice were treated from day 0 and accompanying body weights are shown (mean ± SD). For **B**, **E**, and **F**, *, $P < 0.05$; **, $P < 0.01$; ***, $P < 0.001$ (one-way ANOVA).

Europe PMC Funders Author Manuscripts

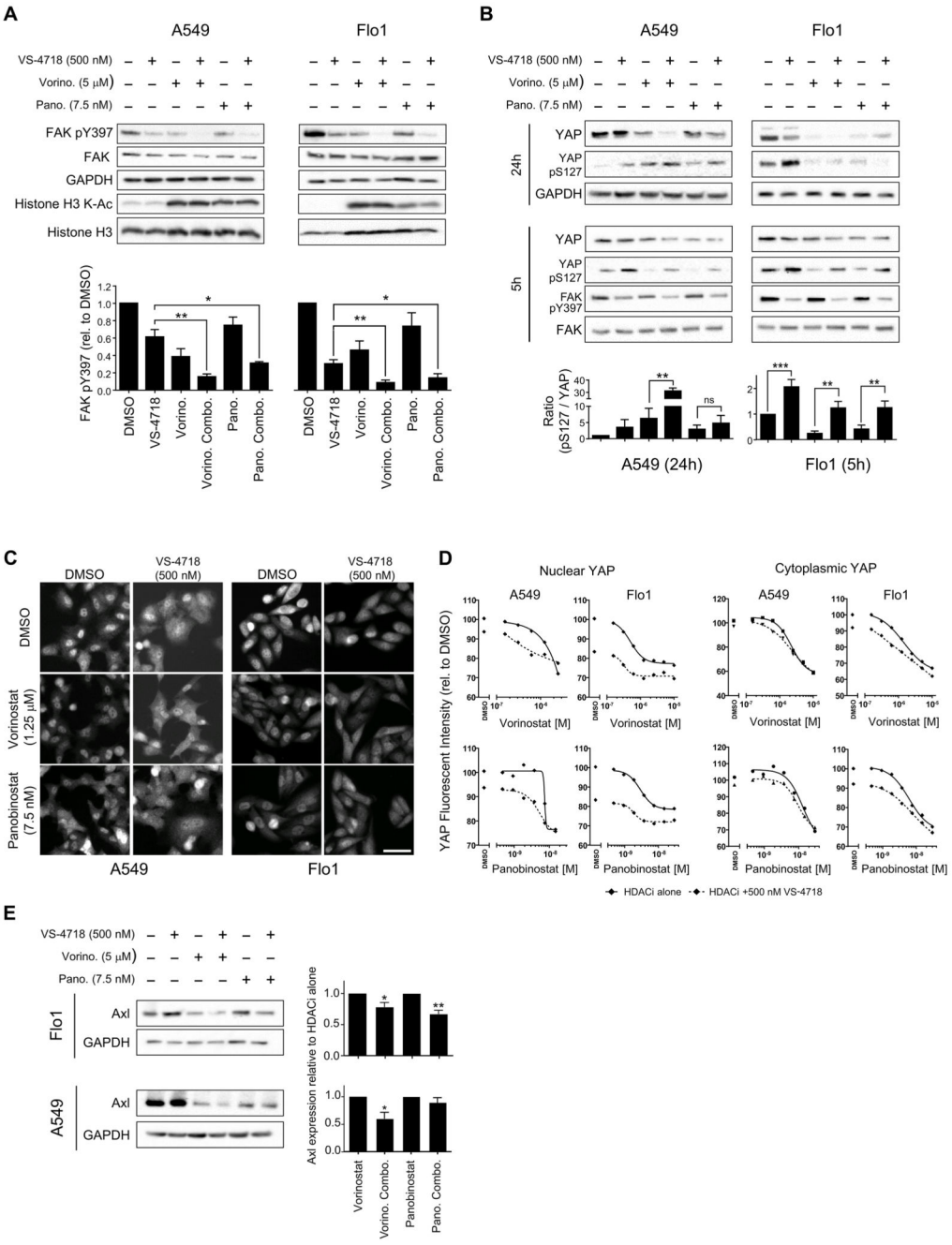

Figure 4. Combined inhibition of HDAC and FAK abolishes FAK kinase activity and regulates YAP localization.

A, Lysates from A549 (left) and Flo1 (right) cells treated as indicated were immunoblotted for FAK, phosphorylated FAK (Y397), GAPDH, histone H3, and acetylated (K-Ac) histone H3. Quantification of phosphorylated FAK (Y397) immunoblotting (bottom) is displayed as means ± SEM ($n = 3$ independent experiments). *, $P < 0.05$; **, $P < 0.01$ (one-way ANOVA). **B**, Lysates from A549 (left) and Flo1 (right) cells were immunoblotted for YAP, phosphorylated YAP (S127), FAK, phosphorylated FAK (Y397), and GAPDH at 5 and 24

Europe PMC Funders Author Manuscripts

hours post drug treatment. **C**, A549 (left) and Flo1 (right) cells were fixed and labeled with anti-YAP antibody after 24 hours of drug treatment. Scale bar, 50 μm. **D**, Quantification of nuclear and cytoplasmic anti-YAP labeling. Relative fluorescence intensity values of anti-YAP labeling in the nuclear (left) and cytoplasmic (right) cellular compartments were normalized to DMSO values and displayed as means ± SEM ($n = 3$ independent experiments). **E**, Lysates from Flo1 (top) and A549 (bottom) cells treated as indicated were immunoblotted for Axl and GAPDH. Quantification of Axl expression is displayed as means ± SEM ($n = 3$ independent experiments). *, $P < 0.05$; **, $P < 0.01$ (one-way ANOVA).

Europe PMC Funders Author Manuscripts

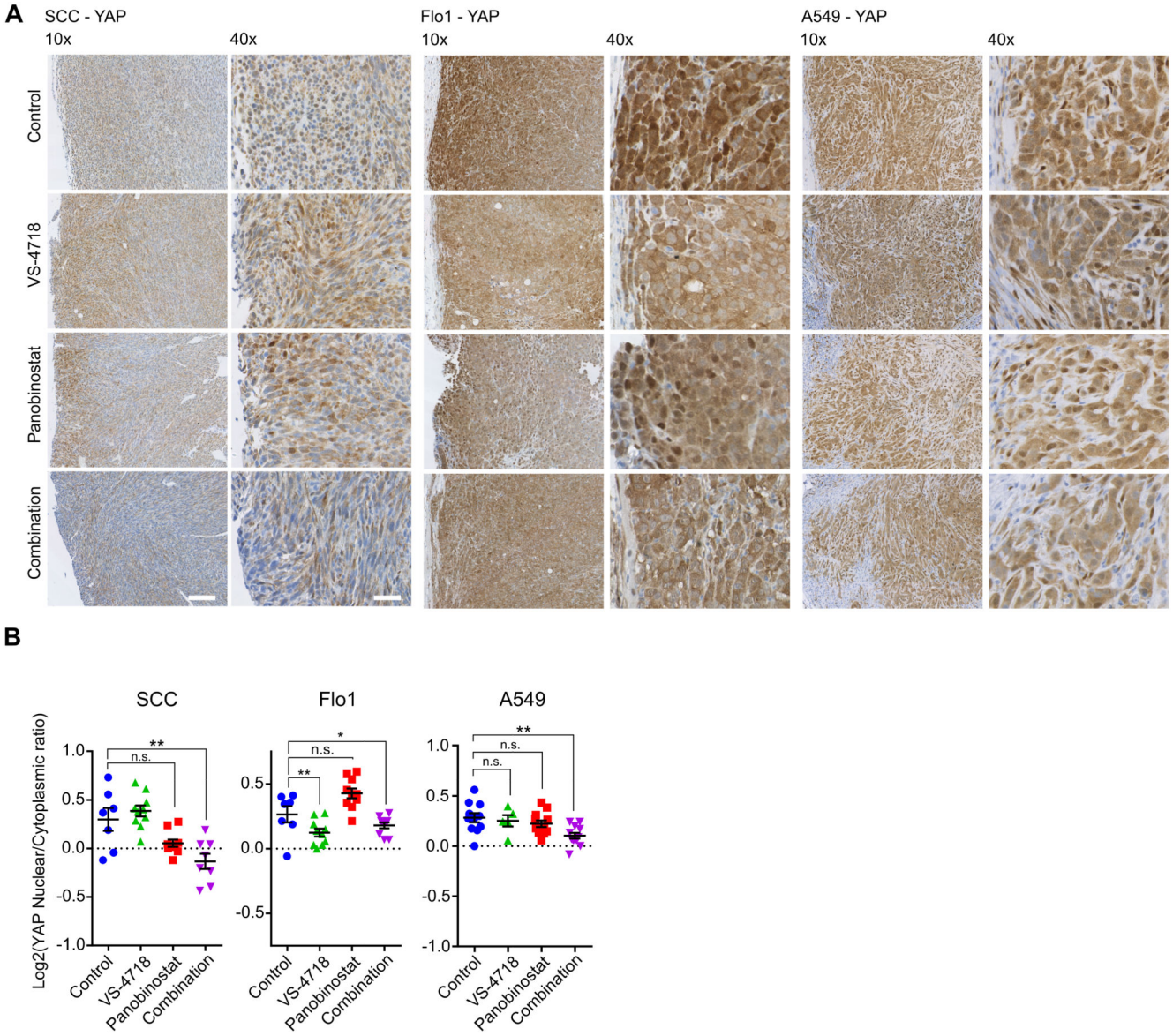

Figure 5. Immunohistochemical analysis of YAP localization in tumors exposed to a FAK and HDAC inhibitor combination.

A, YAP localization was analyzed by immunohistochemistry in SCC (left), Flo1 (middle), and A549 (right) tumors. Tumor sections were labeled with anti-YAP antibody. Scale bar, 100 μm. **B**, Quantification of YAP nuclear/cytoplasmic expression at tumor margins. Each symbol represents the average value per tumor, and horizontal black lines represent group means ± SEM [n ≥ 4 mice per group (2 tumors per mouse)]. *, $P < 0.05$; **, $P < 0.01$; ***, $P < 0.001$ (one-way ANOVA).

Europe PMC Funders Author Manuscripts